



Determination of the Corrosion–Oxidation Turning Point at the Field’s Metal/Chromium Interface by Electrical Contact Resistance Measurement

A. Micallef¹ · C. Stiewe¹ · E. Müller^{1,2}

Received: 5 February 2023 / Accepted: 3 July 2023 / Published online: 31 July 2023
© The Author(s) 2023

Abstract

The correlation of the electrical contact resistance measurement and microanalysis of the Field’s metal (FM)/Cr interface was used to determine the temperature-dependent reactions at the interface. Oxidation of Cr by oxygen contained in FM was identified through a sharp increase of the contact resistance around a certain temperature, above which the following resistance decrease was associated to a corrosion process. The corrosion–oxidation turning point was observed around 390 ± 1.7 °C. Cr saturation in FM combined with complete consumption of the oxygen contained in the FM induced a stabilization of the interface giving a specific contact resistance of about $30 \mu\Omega\cdot\text{cm}^2$.

Keywords Interface · Liquid metal · Field’s metal · Corrosion-oxidation turning point · Specific contact resistance

1 Introduction

Metals or alloys with a melting temperature below 300 °C are classified among the low melting alloys [1]. Multiple applications require the use of such low melting alloys, e. g. wave soldering [2] or characterization techniques, such as the Combined Thermoelectric Measurement technique (CTEM) [3]. Liquid metals represent a corrosive environment; however, unlike corrosion by aqueous solutions involving electro-chemical processes, corrosion by liquid metal relies on a physical–chemical process which is independent of electron transfer through the liquid. In this way, applications containing liquid metal/solid metal interfaces often face issues linked to

✉ A. Micallef
antoine.micallef5@gmail.com

¹ Institute of Materials Research, German Aerospace Center (DLR), 51170 Cologne, Germany

² Institute for Inorganic and Analytical Chemistry, Justus Liebig University Giessen, Heinrich-Buff-Ring 17, 35392 Giessen, Germany

mass transfer corrosion. Investigations about low melting alloys for use as coolants for nuclear power plants alternatively revealed oxidation or dissolution of the metal pipes [4]. The corrosion–oxidation turning point was identified by monitoring the pipes weight evolution along annealing. Weight gain was interpreted as caused by oxidation, while weight loss was the consequence of corrosion. The corrosion–oxidation balance at the liquid metal/solid metal interface depends on time, temperature, oxygen concentration in the liquid, liquid flow, chemical compositions and elemental solubility of the solid metal in the liquid metal. The determination of the corrosion–oxidation turning point is crucial to set the application temperature range.

Recently, a newly designed facility, named Contact Resistance In-Situ monitoring (CoRIS), was demonstrated to trace the oxidation progress versus temperature at the Field’s metal (FM)/FeSi₂ interface via its effect on the contact resistance [5]. The CoRIS technique thus turned out to be a powerful tool to detect the corrosion–oxidation turning point at liquid metal/solid conductor interfaces. Chromium is commonly used as a corrosion protection, e.g. in stainless steel [6]; nevertheless, the corrosion resistance of chromium can be limited in certain conditions [4]. Introducing Cr at the FM/FeSi₂ interface could be a solution to prevent the formation of interface oxides increasing the electrical contact resistance. On the other hand, due to the low toxicity of its constituents, FM is a good surrogate for conducting comparative experiments on coolants for nuclear plant pipes made of Cr-containing steels [7]. In this way, this specific study aimed for determining the corrosion–oxidation turning point of pure Cr soldered with commercial FM using the CoRIS.

2 Materials and Methods

Chromium blocks were supplied by Thermo Fisher Scientific, Karlsruhe, Germany with a size of 6.35×6.35×6.35 mm³ and a purity of 99.95 %. The temperature-dependent resistivity of Cr is known as $\rho_{Cr}(T) = (1.04 \times 10^{-5} + 4.58 \times 10^{-8} T \cdot K^{-1}) \Omega \cdot m$ [8]. Due to high stability of chromium(III) oxide (Cr₂O₃) [9], Cr is often added in alloys, such as stainless steels, to form a passivation layer and prevent corrosion. FM (supplied by Rotometals, San Leandro, USA) is a eutectic low melting alloy with the composition Bi:In:Sn = 32.5:51:16.5 in wt % [10]. FM contains three phases at room temperature: In₂Bi, β -In_{1-x}Sn_x (In-rich), γ -In_{1-x}Sn_x (Sn-rich), and has a melting point of 62 °C [11]. EDX analysis revealed that the as-received FM contained about 20 at. % of oxygen.

To measure the contact resistance at the Cr/FM interface, the CoRIS requires the mounting of an assembly consisting of chromium blocks pairwise soldered with FM (Fig. 1a, c). The mounting protocol of the assembly starts by grinding the contact surfaces of the blocks with SiC abrasive paper to the grit size of P4000. The Cr blocks are then cleaned in ethanol in an ultrasonic bath. Subsequently, they are heated on a hot plate above the melting temperature of the solder, i.e. above 62 °C, in open air. FM pieces are put on top of both contact surfaces, melted and spread mechanically over the contact surfaces using a thin wooden tip as a tool to assist wetting of the metal surface by the liquid solder. The pre-soldered surfaces of the Cr blocks are attached to each other and loaded with a pressure of about 30 kPa. Then the solder solidifies during

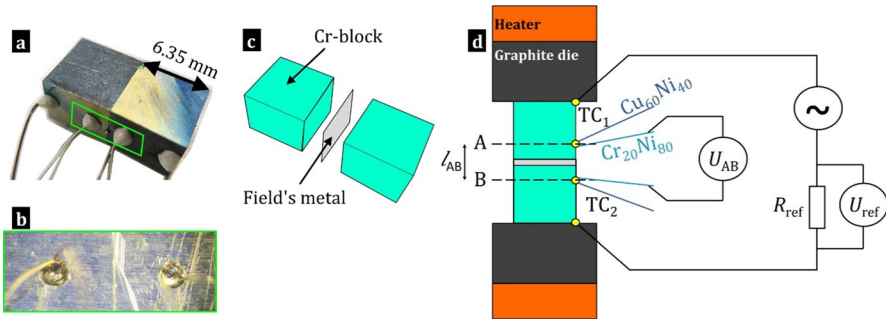


Fig. 1 Cr/FM/Cr assembly and measurement principle of the CoRIS. (a) Photograph of assembly 1 (Table 1) after cycle 1 in the CoRIS. The wires are welded first and then fixed by a ceramic adhesive. (b) The current and signal wires for the measurement are laser-welded to the block’s envelope face. (c) Exploded view of the contact scheme of the assembly. (d) Schematic of the assembly and electrical circuits in the CoRIS containing thermocouples (TC) and signal leads for temperature and resistance monitoring

passive cooling. As a next step, the assembly is equipped with current leads and type E thermocouples which are attached by laser welding at a distance of about 2 mm from the contact face (Fig. 1a, b). High-temperature resistant ceramic paste (CC high temp cement, OMEGA, Stamford, USA) was applied to the wiring connection points as a mechanical support (Fig. 1a). Using the same procedure, two separate assemblies were prepared for the CoRIS measurement in order to test two different temperature regimes as described below (Table 1).

The custom-built CoRIS facility [5] was developed to evaluate the temperature dependence of the electrical contact resistance under thermal cycling. The assembly is vertically inserted between two graphite dies specially designed to keep the Cr blocks geometrically aligned while the solder is in the liquid state. Both graphite dies are connected to heaters, see Fig. 1d, allowing for a temperature dependent measurement of the assembly up to 575 °C in a high vacuum ($\approx 10^{-4}$ mbar). The accuracy limit of the temperature measurement is 1.7 K, which is the standard uncertainty of type-E thermocouples [12].

As shown in Fig. 1d, ohmic voltage pick-up in the 4-point resistance measurement and temperature monitoring is performed via thermocouples (TC₁, TC₂) welded to the Cr blocks. A current is supplied to the assembly via external signal leads. AC of around 50 mA at a frequency of 777 Hz was sent through the assembly. The current I is obtained from the voltage U_{ref} over the reference resistance R_{ref} in the circuit by

Table 1 Cycling regimes in the CoRIS for the investigated assemblies

<i>Assembly #</i>	1	2	2	2
<i>Cycle #</i>	1	1	2	3
<i>Heating rate</i>	5 K·min ⁻¹	5 K·min ⁻¹	5 K·min ⁻¹	5 K·min ⁻¹
<i>Target temperature</i>	575 °C	350 °C	520 °C	575 °C
<i>Holding time</i>	1 h	15 min	3 h	15 min

Bold fonts indicate the assembly number to which the temperature cycles were performed

Ohm's law. The resistance R_{AB} between TC_1 and TC_2 is obtained from the corresponding ohmic voltage, U_{AB} , and I (Eq. 1).

$$R_{AB} = U_{AB}/I, \quad \text{with} \quad I = U_{ref}/R_{ref} \quad (1)$$

Assuming a symmetric configuration, R_{AB} depends on two contributions: Cr block resistance R_{Cr} , twice the contact resistance induced by the Cr/FM interface (R_c). Due to its small contribution (about $2 \mu\Omega$), the solder resistance is neglected.

$$R_{AB} = R_{Cr} + 2R_c \quad (2)$$

Considering the thickness of the solder layer negligible, R_{Cr} is calculated via the thermocouple distance l_{AB} (Fig. 1d), assembly cross section A_c and chromium electrical resistivity ρ_{Cr} . In this way, R_c can be expressed as

$$R_c = \frac{R_{AB} - R_{Cr}}{2}, \quad \text{with} \quad R_{Cr} = \frac{\rho_{Cr} \cdot l_{AB}}{A_c}. \quad (3)$$

The specific contact resistance (r_c) is calculated using the contact area A_c .

$$r_c = R_c \cdot A_c \quad (4)$$

Throughout the measurement, resistance and temperatures are continuously recorded. The heating rate was set to $5 \text{ K}\cdot\text{min}^{-1}$ from room temperature to target temperature. The holding phase duration at maximum temperature was varied between cycles and between assemblies (Table 1). The passive cooling required approximately eight hours from $575 \text{ }^\circ\text{C}$ down to room temperature.

After a temperature cycle sequence, one side of the sample assembly was ground with SiC paper at the envelope face near the interface to remove a surface layer of a few micrometers and then polished with oxide polishing suspension in order to analyze the microstructure of the contact cross section. The polished surface was imaged by a scanning electron microscope (SEM) ZEISS Ultra 55 equipped with an energy dispersive X-ray spectroscopy (EDX) detector to perform elemental analysis.

3 Results and Discussions

Two different temperature regimes were applied to assemblies 1 and 2 (Table 1). Assembly 1 went through a single temperature cycle up to $575 \text{ }^\circ\text{C}$ with a holding phase of one hour. Assembly 2 passed through a sequence of three dissimilar temperature cycles up to 350 , 520 and $575 \text{ }^\circ\text{C}$, respectively, with holding phases of fifteen minutes (cycles 1 and 3) or three hours (cycle 2). Assembly 2 was dismantled from the CoRIS between cycles 1 and 2.

In Fig. 2 the specific contact resistance of assembly 1 is plotted over temperature for a single temperature cycle (Table 1). The heating phase revealed various and sudden slope changes in the temperature dependence of the specific contact resistance $r_c(T)$ suggesting significant evolution at the contact interface affecting the electrical conductance. $r_c(T)$ showed a slight and progressive increase above the melting

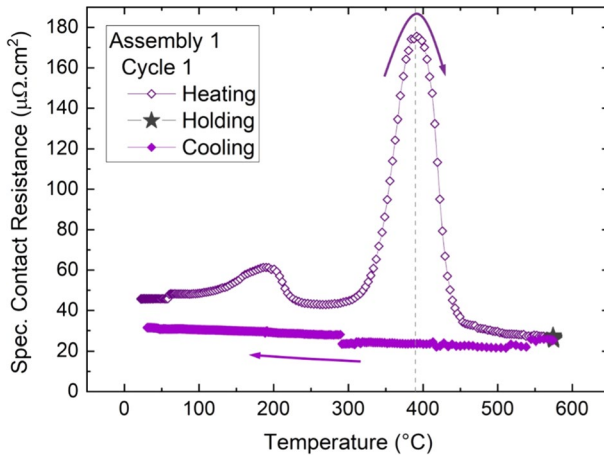


Fig. 2 Specific contact resistance of assembly 1 measured in the CoRIS over a single temperature cycle

temperature of FM. Formation of oxides on liquid metal surfaces, also named dross, is a common phenomenon in soldering processes which might affect the quality of the electrical contact. Jeon et. al stated that the dross formation on an In-activated Ag-Sn-Bi solder was governed by the oxidation of indium [13] due to a higher stability of the indium oxide In_2O_3 compared to the oxides of the other solder components [9]. Therefore, it is assumed that indium might also rule the oxidation process in FM solder forming In-based oxides with the composition $\text{In}_{2-x-y}\text{Sn}_x\text{Bi}_y\text{O}_3$ (with $x+y < 2$). The Bi- and/or Sn-doped In oxides are transparent conductive oxides (TCOs) with low resistivities in the range of $10^{-3} \Omega \text{ cm}$ [14, 15]; in this range, dross of FM should not significantly affect the contact resistance at the Cr/FM interface. Nevertheless, the dross growth increases the surface tension of the solder [1] inducing a wetting degradation of the solder and thus of the electrical contact [16]. The increase of contact resistance starting at 62 °C (Fig. 2) can then be attributed to the formation of solder oxide on the liquid metal surface [17, 18]. Above 190 °C the contact resistance turned to decrease again, which indicates that the dross growth tended to stabilize while resistivities of TCOs decrease with temperature up to about 250 °C [19]. Subsequently, the specific contact resistance remained stable around 40 $\mu\Omega\text{-cm}^2$ between 230 °C and 300 °C. Above 300 °C, the specific contact resistance steeply increased up to 175 $\mu\Omega\text{-cm}^2$ at 390 °C and sharply dropped to approx. 30 $\mu\Omega\text{-cm}^2$ at 450 °C forming a peak shape. The contact resistance increase at the peak could be a consequence of oxidation at the interface, while the following decrease would suggest a degradation of the oxide layer due to corrosion. During the holding phase, the specific contact resistance remained constant around 25 $\mu\Omega\text{-cm}^2$ at 575 °C. During the cooling phase the specific contact resistance remained almost constant with final values of around 30 $\mu\Omega \text{ cm}^2$ at 30 °C.

The cycling regime of assembly 2 (Table 1) was designed to dissect the resistance peak observed at 390 °C in the heating curve of assembly 1 (Fig. 2). As shown in Fig. 3, the first temperature cycle of the assembly 2 was set to a target

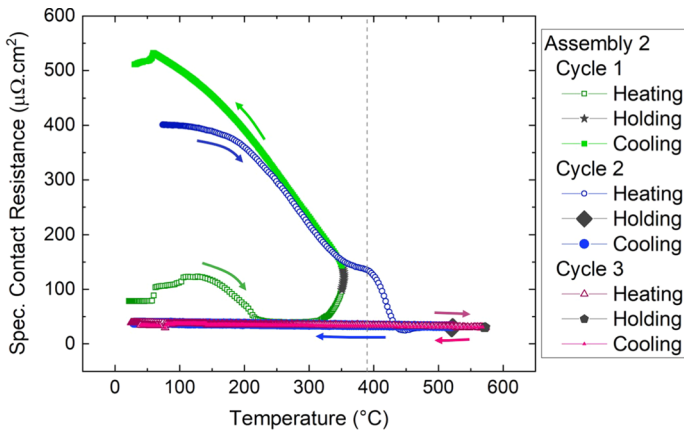


Fig. 3 Specific contact resistance of assembly 2 measured over three temperature cycles in the CoRIS. Empty colored symbols represent the heating phases, while grey and colored filled symbols describe the holding phases and the cooling phases, respectively

temperature of 350 °C. Below 300 °C, the heating phase of cycle 1 showed the same resistance behavior as observed on assembly 1 except that the saturation of the dross growth was monitored earlier, i.e. the contact resistance started to decrease at 130 °C (Fig. 3) compared to 200 °C (Fig. 2). Benamati et al. observed that Cr-containing steels plunged in liquid Bi-Pb led to oxidation of chromium from 300 °C on [20]. Chromium oxide, Cr_2O_3 , is more stable than In-based oxides [9]; therefore, above 300 °C, chromium reduced the In-based oxides and the specific contact resistance abruptly increased due to the high resistivity of Cr_2O_3 ($1.3 \times 10^3 \Omega\text{-cm}$ [21]). Subsequently, the specific contact resistance continued to increase during the holding phase ($5.64 \mu\Omega\text{-cm}^2\text{-min}^{-1}$) indicating the growth of the Cr_2O_3 layer at the FM/Cr interface. During the cooling phase, the contact resistance continuously increased, which is in agreement with the resistivity's temperature trend of Cr_2O_3 [22]. Between cycles 1 and 2, the assembly 2 was dismounted from the measurement device; this manipulation might have led to a slightly different mechanical load distribution on the sample causing a lower specific contact resistance value at the start of cycle 2 ($400 \mu\Omega\text{-cm}^2$ at 75 °C) compared to that monitored at the end of cycle 1 ($520 \mu\Omega\text{-cm}^2$ at 75 °C). Nevertheless, the heating resistance curve of cycle 2 met the cooling resistance curve of cycle 1 around 200 °C. Around 340 °C, the slope of the heating resistance curve of cycle 2 flattened, indicating that Cr oxidation restarted. Similar to assembly 1 (Fig. 2), the specific contact resistance dropped above 390 °C corresponding most likely to the corrosion–oxidation turning point of the FM/Cr interface.

As mentioned in the introduction, Cr containing steels faced similar corrosion–oxidation turning points when plunged into liquid Pb-based alloys during annealing between 300 °C and 600 °C. Indeed, annealing at 470 °C showed that oxide layers were formed on the steel samples protecting them against liquid metal corrosion [23]. On the other hand, for annealing temperature at 550 °C, the

steel samples faced strong corrosion. At high temperature, oxidation and mass transfer corrosion compete at the solder/steel interface. At the temperature of the corrosion–oxidation turning point, the mass transfer by corrosion starts to dominate the process inducing a degradation of the superficial oxide and the dissolution of steel into the liquid metal [24].

A very similar process can be assumed for the Cr/FM interface. Indeed, when the Cr/FM interface reached 390 °C (Figs. 2 and 3), the degradation of the insulating Cr_2O_3 layer led to a direct contact between FM and pure Cr, thus to a reduction of the contact resistance. The resistance heating curve of cycle 2 flattened around 450 °C and revealed an almost constant specific contact resistance around $30 \mu\Omega\cdot\text{cm}^2$ until the end of the holding phase which lasted three hours at 520 °C. The cooling phase of cycle 2, as well as the entire cycle 3, showed that the specific contact resistance of the Cr/FM interface remained always below $40 \mu\Omega\cdot\text{cm}^2$. This suggests that oxygen, initially contained in the solder, was fully consumed after cycle 2 and that Cr oxide degradation was completed around 450 °C during the heating phase of cycle 2.

As shown in Figs. 2 and 3, the corrosion–oxidation turning point at the FM/Cr interface was monitored around 390 °C, i.e. chromium dissolved into the solder above this temperature. The corrosion of Cr was confirmed by subsequent microstructure investigations which revealed a rough contact surface of Cr at the Cr/FM interface (Fig. 4) and also a small amount of chromium in the solder for both assemblies (about 1.5 at. %). Although no value for the solubility limit was found in literature, few authors mentioned chromium solubility in indium, which represents 51 wt % of FM. Among them, Raman et al. stated that indium dissolves Cr “surprisingly well” [25]. In this way, it can be assumed that Cr can be significantly dissolved into FM. Nevertheless, due to the small amount of FM at the interface (Fig. 4) the liquid FM should be rapidly Cr-saturated. As shown in Figs. 2 and 3, the specific contact resistance of the Cr/FM interface stabilized above 450 °C, which suggests that the breaking of the lowly conducting oxide layer is either complete or stopped because FM became Cr-saturated above this temperature.

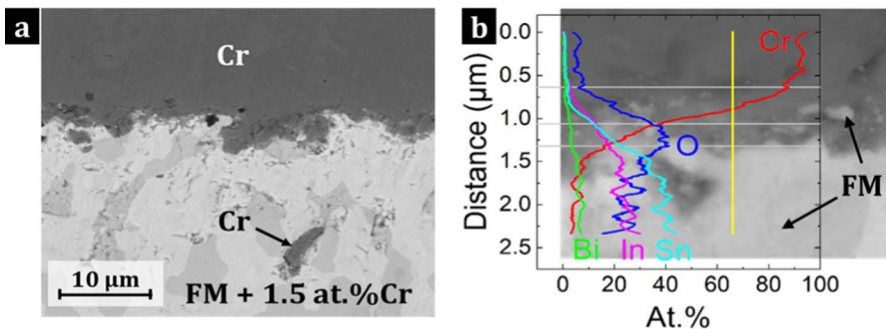


Fig. 4 Backscattered images of the contact cross section for assembly 1 after temperature cycling. (a) Microstructure of the Cr/FM interface. (b) Line scan over the Cr/FM interface

The EDX line scan in Fig. 4b revealed a peak of oxygen at the Cr/FM interface suggesting the presence of residual oxide at the Cr/FM interface. This observation agrees to the previous conclusions stating that the contact resistance increase below 390 °C was associated to the Cr surface oxidation. Above 390 °C, corrosion dominates the oxidation leading to a degradation of the Cr oxide layer. As shown in Fig. 4b, the microstructure at the oxygen peak location contains traces of solder (light grey) which indicates a degraded and hence permeable oxide layer. As shown in Fig. 4a, b, thin and darker elongated particles are visible in the solder close to the FM/Cr interface. Above 300 °C, the initial content of oxygen in the solder reacted with Cr to form numerous small phase inclusions of Cr oxides, which, after degradation above 390 °C, would be enclosed as isolated debris in the solder, but not anymore as a coherent, resistance-increasing oxide layer at the Cr/FM interface as before the beginning of the corrosion period. Due to a limited spatial resolution of 2 μm of the EDX, the nanosized dimension of the oxide debris did not allow a clear identification in its chemical composition.

4 Conclusion

The current study focused on the physical and chemical reactions occurring at the interface between chromium and a low-melting solder (Field's metal) during temperature cycling. These reactions could be interpreted via a temperature-dependent *in-situ* contact resistance measurement. From 300 °C on, oxidation is dominating and is forming a closed Cr oxide layer on the Cr surface at the Cr/FM interface. Hence the contact resistance rises, due to the low conductivity of Cr oxide. In addition, the formed oxide layer protects Cr from corrosion.

At higher temperatures, a resistance drop, initiated at 390 °C, is observed when the coherent layer breaks. As a consequence, the FM comes into direct contact to the Cr surface, allowing at the same time the dissolution of metallic Cr into the solder. This transition corresponds to the corrosion–oxidation turning point from which on Cr corrosion by FM dominates the previous oxidation process. The observation of isolated Cr particles in the FM is a proof of the described mechanism of the corrosion process which may follow cracks or grain boundaries in the bulk Cr.

As soon as Cr is dissolving, oxidation of dissolved Cr atoms in the solder will have preference over surface oxidation as it will not require transport of oxygen via diffusion and convection to the interface. In this way, the reaction can happen everywhere in the melt where Cr and oxygen meet. Thus, the remaining oxygen in the melt should have been rapidly consumed at this point.

Corrosion of Cr causes the degradation of the insulating Cr oxide layer formed below 390 °C which ends up as isolated debris enclosed in the liquid solder. Above 390 °C, FM was rapidly saturated by Cr and the remaining oxygen was quickly consumed, thus stabilizing the degrading Cr/FM interface. After heating up to 520 °C (cycle 2 in Fig. 3), the specific contact resistance of the Cr/FM interface remained constant around 30 μΩ·cm² between room temperature and 575 °C.

Acknowledgements The authors would like to thank Gregor Oppitz for his technical support on the CoRIS facility. A. Micallef would like to thank the German Academic Exchange Service (DAAD) for the endorsement (DLR-DAAD scholarship—fellowship no. 247).

Author Contributions AM wrote the main manuscript text and prepared all figures. C. Stiewe and E. Müller participated in the results analysis and supervised the overall content production. All authors reviewed the manuscript.

Funding Open Access funding enabled and organized by Projekt DEAL. German Academic Exchange Service (DAAD) funded the DLR-DAAD scholarship (fellowship no. 247) enabling A. Micallef to complete this study.

Data Availability This declaration is not applicable.

Declarations

Competing interests We declare that the authors have no competing interests as defined by Springer, or other interests that might be perceived to influence the results and/or discussion reported in this paper.

Open Access This article is licensed under a Creative Commons Attribution 4.0 International License, which permits use, sharing, adaptation, distribution and reproduction in any medium or format, as long as you give appropriate credit to the original author(s) and the source, provide a link to the Creative Commons licence, and indicate if changes were made. The images or other third party material in this article are included in the article's Creative Commons licence, unless indicated otherwise in a credit line to the material. If material is not included in the article's Creative Commons licence and your intended use is not permitted by statutory regulation or exceeds the permitted use, you will need to obtain permission directly from the copyright holder. To view a copy of this licence, visit <http://creativecommons.org/licenses/by/4.0/>.

References

1. H.R. Kotadia, P.D. Howes, S.H. Mannan, A review: on the development of low melting temperature Pb-free solders. *Microelectron. Reliab.* **54**(6–7), 1253–1273 (2014)
2. A. Forstén, H. Steen, I. Wilding, J. Friedrich, Development and validation of lead-free wave soldering process. *Solder. Surf. Mt. Technol.* **12**, 29–34 (2000)
3. H. Kolb, T. Dasgupta, K. Zbrocki, E. Müller, J. de Boor, Simultaneous measurement of all thermoelectric properties of bulk materials in the temperature range 300–600 K. *Rev. Sci. Instrum.* **86**, 073901 (2015)
4. J. Zhang, N. Li, Analysis on liquid metal corrosion–oxidation interactions. *Corros. Sci.* **49**, 4154–4184 (2007)
5. A. Micallef, C. Stiewe, G. Oppitz, E. Müller, High-temperature specific contact resistance of iron disilicide soldered to molybdenum by field's metal. *ACS Appl. Electron. Mater.* **3**, 890–897 (2021)
6. N.R. Baddoo, B. Burgan, *Structural Design of Stainless Steel* (The Steel Construction Institute, London, 2001), p.130
7. A. Lipchitz, L. Laurent, G. D. Harvel, Suitability of eutectic field's metal for use in an electromagneto-hydrodynamically-enhanced experimental two-phase flow loop, in *International Conference on Nuclear Engineering*, vol. 44991 (American Society of Mechanical Engineers, Anaheim, 2012), pp. 51–58
8. H. P. R. Frederikse. Section 12: Properties of solids, in *CRC Handbook of Chemistry and Physics*, ed. by D.R. Lide, 84th ed. (CRC Press, Boca Raton, 2004), pp. 1–233
9. H.J.T. Ellingham, Reducibility of oxides and sulphides in metallurgical processes. *J. Soc. Chem. Ind.* **63**, 125–133 (1944)
10. S. Akbulut, Y. Ocak, N. Maraşlı, K. Keşlioğlu, H. Kaya, E. Çadırılı, Determination of solid–liquid interfacial energies in the In–Bi–Sn ternary alloy. *J. Phys. D Appl. Phys.* **41**, 175302 (2008)

11. M. Kamal, A. El-Bediwi, R.M. Shalaby, M. Younus, A study of eutectic indium-bismuth and indium-bismuth-tin Field's metal rapidly solidified from melt. *J. Adv. Phys.* **7**, 1404–1413 (2015)
12. G.W. Burns, M.G. Scroger, G.F. Strouse, M.C. Croarkin, W.F. Guthrie, *NIST Monograph 175: Temperature-Electromotive Force Reference Functions and Tables for the Letter-Designated Thermocouple Types Based on the ITS-90* (National Institute for Standard Technology, Washington, 1993), p.630
13. A.-J. Jeon, S.-J. Kim, S.-H. Lee, C.-Y. Kang, Effect of indium content on the melting point, dross, and oxidation characteristics of Sn–2Ag–3Bi–xIn solders. *J. Electron. Packag.* **135**, 0210061–0210065 (2013)
14. S. Noguchi, H. Sakata, Electrical properties of undoped In₂O₃ films prepared by reactive evaporation. *J. Phys. D Appl. Phys.* **13**, 1129 (1980)
15. R. Bel Hadj Tahar, T. Ban, Y. Ohya, Y. Takahashi, Tin doped indium oxide thin films: electrical properties. *J. Appl. Phys.* **83**, 2631–2645 (1998)
16. N. Eustathopoulos, M.G. Nicholas, B. Drevet, Fundamental equations of wetting, in *Wettability at High Temperatures*, vol. 3, ed. by R.W. Cahn (Elsevier, Oxford, 1999), pp.1–53
17. Y. Liu, W. Manning, B. Huang, N.-C. Lee, *A Model Study of Profiling for Voiding Control at Lead-Free Reflow Soldering* (Clinton, 2005)
18. D.-S. Kim, Q. Yu, T. Shibutani, N. Sadakata, T. Inoue, Effect of void formation on thermal fatigue reliability of lead-free solder joints, in *The 9th Intersociety Conference on Thermal and Thermomechanical Phenomena In Electronic Systems (IEEE Cat. No. 04CH37543)*, vol. 2 (IEEE, 2004), pp. 325–329
19. Y. Hu, X. Diao, C. Wang, W. Hao, T. Wang, Effects of heat treatment on properties of ITO films prepared by rf magnetron sputtering. *Vacuum* **75**, 183–188 (2004)
20. G. Benamati, C. Fazio, H. Piankova, A. Rusanov, Temperature effect on the corrosion mechanism of austenitic and martensitic steels in lead–bismuth. *J. Nucl. Mater.* **301**, 23–27 (2002)
21. W. Martienssen, H. Warlimont, *Springer Handbook of Condensed Matter and Materials Data* (Springer, Berlin, 2006), p.1119
22. M.D. Julkarnain, J. Hossain, K.S. Sharif, K.A. Khan, Temperature effect on the electrical properties of chromium oxide (Cr₂O₃) thin films. *J. Optoelectron. Adv. Mater.* **13**, 485 (2011)
23. F. Balbaud-Celerier, P. Deloffre, A. Terlain, A. Rusanov, Corrosion of metallic materials in flowing liquid lead-bismuth. *J. Phys. IV Fr.* **12**, 177–190 (2002)
24. J. Zhang, N. Li, Y. Chen, A.E. Rusanov, Corrosion behaviors of US steels in flowing lead–bismuth eutectic (LBE). *J. Nucl. Mater.* **336**, 1–10 (2005)
25. A. Raman, K. Schubert, UBER DEN AUFBAU EINIGER ZU TIAL₃ VERWANDTER LEGIERUNGSREIHEN. 2. UNTERSUCHUNGEN IN EINIGEN T-AL-SI UND T4...6-IN-SYSTEMEN. *Z. Metall.* **56**, 44–52 (1965)

Publisher's Note Springer Nature remains neutral with regard to jurisdictional claims in published maps and institutional affiliations.